FEBS Letters 589 (2015) 1200–1206

journal homepage: www.FEBSLetters.org

Crystal structure of an acetylesterase from *Talaromyces cellulolyticus* and the importance of a disulfide bond near the active site

Masahiro Watanabe [a], Harumi Fukada [b], Hiroyuki Inoue [a], Kazuhiko Ishikawa [a,*]

[a] Biomass Refinery Research Center, National Institute of Advanced Industrial Science and Technology (AIST), 3-11-32 Kagamiyama, Higashi-Hiroshima, Hiroshima 739-0046, Japan
[b] Graduate School of Life and Environmental Sciences, Osaka Prefecture University, 1-1 Gakuen-cho, Nakaku, Sakai, Osaka 599-8531, Japan

ARTICLE INFO

Article history:
Received 15 January 2015
Revised 10 March 2015
Accepted 17 March 2015
Available online 28 March 2015

Edited by Miguel De la Rosa

Keywords:
Biomass
Carbohydrate esterase
Catalytic triad
Disulfide bond
Saccharification
Xylanase

ABSTRACT

Carbohydrate esterase catalyzes the de-*O* or de-*N*-acylation of substituted saccharides in plant cell walls and thus has great potential for industrial biomass saccharification. We recently identified the putative carbohydrate esterase family 3 (CE3) from *Talaromyces cellulolyticus*. Here, we prepared the recombinant catalytic domain of the enzyme and crystallized it. The crystal structure was determined to 1.5 Å resolution. From the structural analysis, it was elucidated that a n-octyl-β-D-glucopyranoside bound to near the catalytic triad (Ser10, Asp179 and His182) and was buried in the active site cavity. Site-directed mutagenesis showed that the N-terminal disulfide bond located near the catalytic triad is involved in the activity and structural stability of the enzyme.

1. Introduction

Lignocellulosic biomass, the most abundant source of carbon on earth, consists of a highly complicated macromolecular structure comprising various carbohydrate polymers in the plant cell wall [1–3]. The microbial degradation of the plant cell wall is an effective biological process [4–5] that is also of industrial interest for the production of biofuels and biomaterials [6]. However, most of the cell wall polysaccharides, including xylan, mannan and glucomannan, are largely acetylated (or acylated), which sterically inhibits the access of glycoside hydrolases, preventing attack of the glycosidic linkages in the polysaccharides [7]. Consequently, removal of the acetylated moieties by carbohydrate esterases could accelerate the degradation of polysaccharides through the action of glycoside hydrolases [7]. The CAZy database (http://www.cazy.org/Carbohydrate-Esterases.html) [8] currently categorizes carbohydrate esterases (CEs) into 16 families (CE1–16). The enzymes in all 16 families display a typical α/β hydrolase fold (except for CE4, which folds into a $(\beta/\alpha)_7$ barrel [9]) and function as serine esterases through a catalytic triad (Ser–His–Asp) [10–15]. Despite their shared α/β hydrolase fold, these esterases show differences in structural details, substrate recognition, and sequence homology. Carbohydrate esterase family 3 (CE3 (EC 3.1.1.72)) enzymes are known as acetylxylan esterases and hydrolyze the ester bond between acetic acid and hemicellulose in plant biomass. The hydrolytic activity of major cellulases such as cellobiohydrolases and endo-type xylanases toward the biomass is enhanced by the reactivity of CE3 [16]. The putative physiological role of CE3 in fungus is to produce the suitable substrate for glycoside hydrolases from lignocellulosic biomass by the esterase activity. Recently, the crystal structure of a bacterial CE3, CtCes3-1 from *Clostridium thermocellum*, was solved at 1.4 Å resolution [17]. It was reported that CtCes3-1 is an acetyl esterase that exhibits a high specific activity toward acetylated xylan and xylooligosaccharides [17]. However, to date no crystal structure of a CE3 enzyme from fungi has been reported.

A mesophilic fungus, *Talaromyces cellulolyticus* (formerly known as *Acremonium cellulolyticus*), can produce a large amount of various saccharification enzymes [18–19]. Examination of the genome database of *T. cellulolyticus* (unpublished data) resulted in the identification of an ORF encoding a putative CE3. Here, we cloned and expressed the catalytic domain of CE3 from *T. cellulolyticus*, solved

Abbreviations: TcAE206, the catalytic domain of acetylesterase from *Talaromyces cellulolyticus*; DSC, differential scanning calorimetry; pNA, *p*-nitrophenyl acetate; pNB, *p*-nitrophenyl butyrate; pNO, *p*-nitrophenyl octanoate

Author contributions: M.W. and K.I. designed research; M.W., H.F., and H.I. performed research; M.W., H.F., and K.I. analyzed data; M.W. and K.I. wrote the paper.

* Corresponding author. Fax: +81 82 420 8291.
E-mail address: kazu-ishikawa@aist.go.jp (K. Ishikawa).

http://dx.doi.org/10.1016/j.febslet.2015.03.020
0014-5793/

its crystal structure, and examined its mechanism of action using biochemical and structural analyses.

2. Materials and methods

2.1. Materials

p-Nitrophenyl acetate (pNA), *p*-nitrophenyl butyrate (pNB), and *p*-nitrophenyl octanoate (pNO) were purchased from Sigma–Aldrich (St. Louis, MO, USA). All other chemicals were of the highest grade commercially available.

2.2. Cloning, expression and purification of the recombinant TcAE206

cDNA encoding the gene for acetylesterase of *T. cellulolyticus* (*ae*) was amplified by reverse transcription-PCR from *T. cellulolyticus* YP-4 derived from Y-94 chromosomal DNA using primers (ae_F and ae_R) as indicated in Table 1. The gene encoding the catalytic domain of acetylesterase (*ae*206) was reconstructed by PCR by eliminating the signal peptide, linker region and CBM-1 sequences using primers (wt_F and wt_R) as indicated in Table 1. The gene (*ae*206) encoding the catalytic domain of acetylesterase (TcAE206) was cloned into pET-11a (Novagen, Madison, WI, USA) at the *Nde*I and *BamH*I restriction enzyme sites so that the *Nde*I site (CATATG) included the initiator methionine codon. The primers used for mutating TcAE206 residue Ser10, Asp179, His182 and Cys16 to alanine (S10A_F & S10_R, D179A_F & D179A_R, H182A_F & H182A_R, C16A_F & C16A_R) are shown in Table 1. Mutagenesis was carried out using a PrimeSTAR Max Premix mutagenesis kit (TaKaRa, Kyoto, Japan) according to the manufacturer's instructions.

The recombinant enzymes were prepared as reported previously [20]. Briefly, TcAE206 was expressed in *Escherichia coli* BL21 (DE3) cells (Invitrogen, Carlsbad, CA, USA). Cells were suspended and lysed by sonication, followed by centrifugation at 39960×*g* for 30 min at 4 °C. The collected supernatant was applied to a HiTrap Q HP column (GE Healthcare, Little Chalfont, UK) equilibrated in 50 mM Tris HCl, pH 8.5, and eluted with an ascending salt gradient. TcAE206 eluted from the column at approximately 200 mM NaCl. Fractions containing TcAE206 protein were pooled and dialyzed into 20 mM Tris, pH 8.0, 2 M NaCl and applied to a HiTrap Butyl HP column (GE Healthcare) equilibrated in the same buffer. Protein was eluted with a descending salt gradient. As a final step, the eluted protein was added directly to a Superdex 200 16–60 gel filtration column (GE Healthcare) equilibrated in 20 mM Tris HCl, pH 8.0, 50 mM NaCl. The purity of the collected protein from this final step was confirmed to be more than 95% by SDS–PAGE. The purified protein was identified by MALDI-TOF mass spectrometry. The protein concentration was determined using the molar extinction coefficient of 36105 M^{-1} cm^{-1} calculated from the amino-acid sequence [21]. The protein concentration was determined by measuring the absorption at 280 nm. S10A, D179A, H182A and C16A mutants were cloned, expressed and prepared in the same manner as the wild-type protein.

Table 1
Summary of nucleotide primers used in this study.

Primer	Nucleotide sequence (5′ → 3′)
For cDNA construction	
ae_F	ATGAAGCTTTCAGGTTTTGCGCTCTTTGCT
ae_R	AATCCTGCAGGCTACAAGCATTGATAGTAG
For plasmid construction	
wt_F	AATCATATGGTCAAAGTCATGCTGCTCG
wt_R	ATTGGATCCTTAAGAGACGTCCTTGATGAG
S10A_F	CTGCTCGGCGACGCAATTACTGAGATC
S10A_R	GATCTCAGTAATTGCGTCGCCGAGCAG
D179A_F	ATGCTGAGAGACGCAGGTGTCCATCCT
D179A_R	AGGATGGACACCTGCGTCTCTCAGCAT
H182A_F	GACGATGGTGTCGCACCTAACAGCAAG
H182A_R	CTTGCTGTTAGGTGCGACACCATCGTC
C16A_F	ACTGAGATCACCGCATGGAGACCACTTG
C16A_R	CAAGTGGTCTCCATGCGGTGATCTCAGT

2.3. Enzymatic activity assay

The activities of the wild-type and mutant catalytic domains were evaluated as reported previously [22] using pNA, pNB and pNO as substrates. Protein solution (1.0 μM; 50 μl) in sodium acetate buffer (pH 5.5) was mixed separately with 0.45 ml of each substrate (1 mM), followed by incubation for 10 min at 50 °C. The amount of released *p*-nitrophenol was determined as the enzymatic activity by measuring the absorption at 405 nm. One unit of AE activity was defined as the amount of enzyme required to liberate 1 μmole of *p*-nitrophenol equivalent per minute at 50 °C. The initial rates of the enzyme reactions (1.0 μM) were measured using substrate concentrations ranging from 0.1 to 10 mM. The Michaelis constant (K_m) and the maximum rate at substrate saturation (V_{max}) were determined by non-linear least squares method [23].

2.4. Optimum temperature and pH measurements

The optimum temperature of TcAE206 was examined in 50 mM MES (pH 6.0). The enzyme solution (1.0 μM) and 1 mM pNA were mixed and reacted for 10 min in a water-bath at 40–85 °C. The optimum pH was determined at 50 °C using, pH 3.0–11.0 buffer [24], followed by incubation with 4 mM pNA for 10 min at 50 °C.

2.5. Crystallization and X-ray data collection

TcAE206 crystals were prepared as previously reported [20]. Briefly, the best TcAE206 crystals were obtained with 170 mM ammonium sulfate, 28% (w/v) PEG 4000, 5% (v/v) glycerol and a final concentration of 0.5% (w/v) n-octyl-β-D-glucopyranoside (β-OG). The optimized drop was prepared by using the hanging-drop vapor diffusion method at 293 K. X-ray diffraction data for TcAE206 crystal was collected at beamline BL44XU at SPring-8 (Hyogo, Japan) using 0.9 Å wavelength radiation. A total of 150° of data were collected using a Rayonix MX225-HE CCD detector. The data were processed to 1.5 Å resolution with HKL2000 (DENZO and SCALEPACK) [25].

2.6. Structure solution and refinement

General data handling was carried out with the CCP4 package [26]. The structures were solved by molecular replacement using PHASER [27] with a search model of CtCes3-1 (PDB # 2VPT). Automated model building was performed using ARP/wARP [28]. Manual adjustment of the models was carried out with COOT [29] and refinement using REFMAC5 [30]. Water molecules were added to the models using ARP/wARP and then manual inspection of the 2*Fo–Fc* and *Fo–Fc* maps. The stereochemical properties of the models were checked with PROCHECK [31] and the validation tools of COOT. Figures were created with CCP4MG [32].

2.7. Differential scanning calorimetry (DSC)

The thermostabilities of TcAE206 and mutants were examined by DSC using a 1.0 mg/ml protein sample in 50 mM sodium acetate, pH 5.5. A nanoDSC instrument (TA Instruments, New Castle, DE, USA) was used and the scanning speed was 1.0 °C per min. Control runs of buffer (no protein) were run before and after each sample run. DSC scans on proteins were performed 2 or 3 times for each protein.

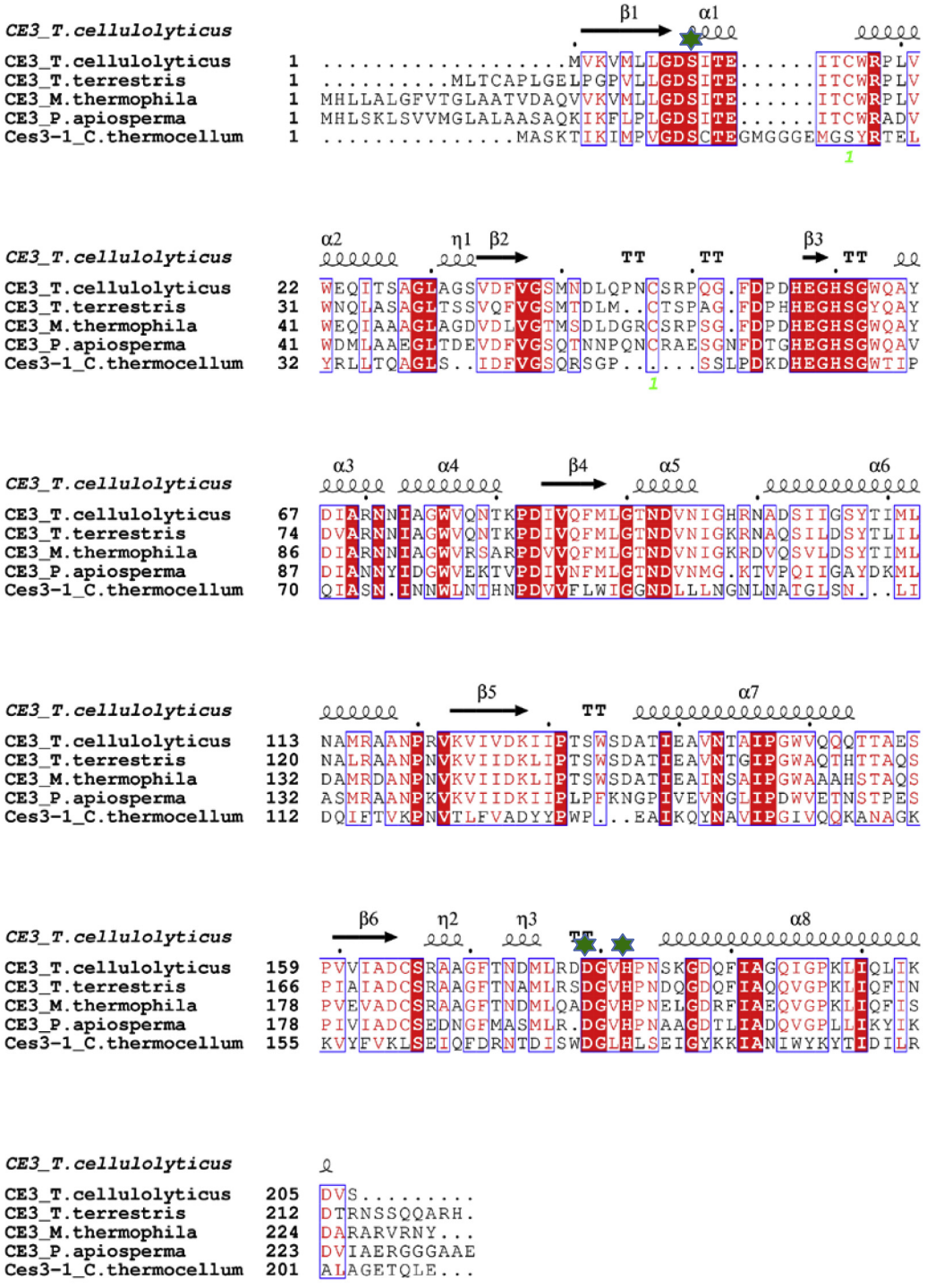

Fig. 1. Structure-based sequence alignment of various CE3 esterases. Strictly conserved residues are boxed in red. Similar residues are written with red characters in blue boxes. The catalytic residues are indicated with green stars. The α-helices (α1–8) and β-strands (β1–6) in TcAE206 are represented as black screws and black arrows, respectively. Two cysteine in regard to the formation of a S—S bond are exhibited as "1" with light green. The species origin of each CE3 is shown by an abbreviation as follows: *T. cellulolyticus*: *Talaromyces cellulolyticus* (GenBank Accession Number BAP90856: the catalytic domain only); *T. terrestris*: *Thielavia terrestris* (GenBank Accession Number XP_003657214); *M. thermophila*: *Myceliophthora thermophila* (GenBank Accession Number XP_003659622); *P. apiosperma*: *Pseudallescheria apiosperma* (GenBank Accession Number KEZ40370); *C. thermocellum*: *Clostridium thermocellum* (GenBank Accession Number ABN52033). The figure was made using ClustalW [38] and ESPript [39].

3. Results and discussion

3.1. Structure-based sequence alignment of TcAE and other CE3 esterases

We identified an ORF encoding a putative CE3 enzyme in the genome data base of *T. cellulolyticus* [33]. The enzyme (TcAE) consists of four components: a putative N-terminal signal peptide, a catalytic core domain, a linker region consisting of a serine/threonine-rich sequence, and a carbohydrate-binding module (CBM-1) at the C-terminus. TcAE206, containing the catalytic domain, has a tightly conserved putative catalytic triad consisting of Ser10, Asp179 and His182 residues in the active site. TcAE206 exhibits approximately 65% sequence identity with other fungal CE3

Table 2
Substrate specificity of TcAE206 toward various *p*-nitrophenol compounds.

Substrate (50 °C)	K_m (mM)	k_{cat}[a] (s^{-1})	k_{cat}/K_m (mM^{-1} s^{-1})
pNA	1.1 ± 0.12	49.2 ± 0.25	44.7 ± 0.25
pNB	7.1 ± 0.16	29.8 ± 0.04	4.1 ± 0.02
pNO	n.d.	n.d.	n.d.

n.d.: not detected.
[a] The turnover value is defined as that rate at which the enzyme can produce *p*-nitrophenol per unit time. The *p*-nitrophenol concentration was determined by using the absorbance at 405 nm. The values of K_m and k_{cat} (mean ± R.M.S.D.) were determined by three independent experiments.

members, especially the acetylxylan esterase family (Fig. 1). However, TcAE206 and other fungal CE3 enzymes exhibit about 20% sequence identity with bacterial CtCes3-1 proteins.

3.2. Optimum pH and temperature of TcAE206

Recombinant TcAE206 was prepared and purified as described in Section 2. The results showed that the optimum pH for enzyme activity is pH 6.0, although the enzyme exhibits some activity at weakly acidic to neutral pH (5.0–8.0). Activity measurements indicated that the optimum temperature for catalysis is 65 °C, and that above 75 °C, activity decreases markedly. There are very few reports pertaining to the optimum pH and temperature of fungal CE3; the present results are the first to show them. Biomass saccharification is more efficient at high temperatures; therefore, we plan in the future to make this enzyme more heat resistant by the protein engineering method based on information obtained from our structural analyses.

3.3. Substrate specificity and kinetics of TcAE206

The experiments showed that the enzyme exhibited by far the highest activity toward pNA, at least fivefold higher than toward pNB or pNO (Table 2, Supplementary Fig. 2), indicating that the activity of the enzyme decreases as the length of the alkyl chain on the substrate increases. These results were obtained using only the catalytic domain (the cellulose-binding module (CBM) is absent); however, the results at least suggest that the catalytic domain exhibits high activity for short-chain acetyl group(s).

Measurement of AE activity showed that the K_m and k_{cat} values of the wild-type catalytic domain for pNA were 1.1 ± 0.12 mM and 49.2 ± 0.25 s^{-1}, respectively, at 50 °C (Table 3). On the other hand, the significant deacetylation activity toward an acetyl xylan extracted from hot-water treated eucalyptus was not detected (data not shown). This result supports the recent report that CE3 does not exhibit the efficient de-esterification activity toward the acetylated xylooligosaccharide as compared with other CE families [34].

Table 3
Kinetic parameters of WT TcAE206 and mutants for pNA.

Enzyme (50 °C)	K_m (mM)	k_{cat}[a] (s^{-1})	k_{cat}/K_m (mM^{-1} s^{-1})
Wild-type	1.1 ± 0.12	49.2 ± 0.25	44.7 ± 0.25
S10A	5.1 ± 0.09	21.8 ± 0.19	4.2 ± 0.07
D179A	1.4 ± 0.08	36.3 ± 0.25	24.8 ± 0.18
H182A	1.8 ± 0.22	38.8 ± 0.11	20.7 ± 0.06
C16A	4.7 ± 0.19	26.2 ± 0.12	5.4 ± 0.03

[a] The turnover value is defined as that rate at which the enzyme can produce *p*-nitrophenol per unit time. The *p*-nitrophenol concentration was determined by using the absorbance at 405 nm. The values of K_m and k_{cat} (mean ± R.M.S.D.) were determined by three independent experiments.

3.4. Overall structure

Recombinant TcAE206 protein was prepared and crystallized as described in Section 2. The crystal structure of TcAE206 was solved at 1.5 Å resolution by molecular replacement method. Data collection and refinement statistics are shown in Table 4.

The crystal structure and amino acid sequence homology of recombinant TcAE206 was typical of the carbohydrate esterase family. The structure of TcAE206 exhibits the SGNH-hydrolase fold comprising five central parallel β-stands (β1, β2, β4, β5, β6) flanked by six α-helices (α2, α3, α4, α6, α7, α8) (Supplementary Fig. 3). The enzyme also has the classic catalytic triad (Ser10–Asp179–His182) of serine esterases, where Ser10 is the nucleophile, His182 is the acid-base, and Asp179 modulates the basic nature of the histidine. The overall structure of TcAE206 closely resembles that of CtCes3-1, with a root mean square deviation (R.M.S.D.) of 1.71 Å (Cα atoms) (Fig. 2) [17]. In common with the majority of this kind of enzymes, the N and C termini are in close proximity, with the first and last residues in the model being separated by approximately 9.6 Å. Comparing the structure of CtCes3-1 has allowed the identification of the active site of the enzyme, which is located above the N-terminal end of the central β-sheet and a number of loops. Fig. 2 shows the speculated active site of TcAE206; the formation of the catalytic triad (Ser–Asp–His) is similar to bacterial CtCes3-1, with R.M.S.D. values of 0.81 Å (Cα atom of Ser), 2.78 Å (Cα atom of Asp) and 0.78 Å (Cα atom of His).

3.5. Structure of the substrate binding pocket

Fig. 2 shows the active site of TcAE206, one disulfide bond formed between Cys16 and Cys47 was observed near the catalytic triad (Ser–Asp–His). The disulfide bond was conserved in other

Table 4
Data collection and refinement statistics.

Data collection	
Wavelength (Å)	0.9
Space group	$P4_12_12$
Unit cell: *a*, *b*, *c* (Å)	*a* = *b* = 70.9, *c* = 87.0
Resolution (Å)	50.0–1.5 (1.53–1.50)[a]
R_{merge}[b] (%)	6.9 (42.0)[a]
Average $I/\sigma(I)$	26.5 (2.3)[a]
Completeness (%)	99.0 (95.8)[a]
Redundancy	6.9 (3.7)[a]
Matthews coefficient ($Å^3$ Da^{-1})	2.62
Solvent content (%)	53.0
No. molecules/asym	1
Refinement	
Resolution (Å)	20.0–1.5
No. reflections (test reflections)	34097 (1789)
R_{work}[c]/R_{free}[d] (%)	18.4/20.7
No. atoms	18554
Protein	17352
Water	1202
Mean overall B factor ($Å^2$)	21.1
Rms deviations	
Bond lengths (Å)	0.02
Bond angles (°)	2.06
Ramachandran plot	
In most favored regions (%)	97.6
In allowed regions (%)	2.0
PDB accession #	3X0H

[a] Outer shell (1.53–1.50 Å).
[b] $R_{merge} = \Sigma_{hkl}\Sigma_i|I_i(hkl) - \langle I(hkl)\rangle|\Sigma_{hkl}\Sigma_i I_i(hkl)$, where $I_i(hkl)$ is the intensity of the *i*th measurement of reflection hkl, including symmetry-related reflections, and $\langle I(hkl)\rangle$ is their average.
[c] $R_{work} = \Sigma_h\Sigma_i||F_o| - |F_c||/\Sigma|F_o|$.
[d] R_{free} is R_{work} for approximately 5% of the reflections that were excluded from the refinement.

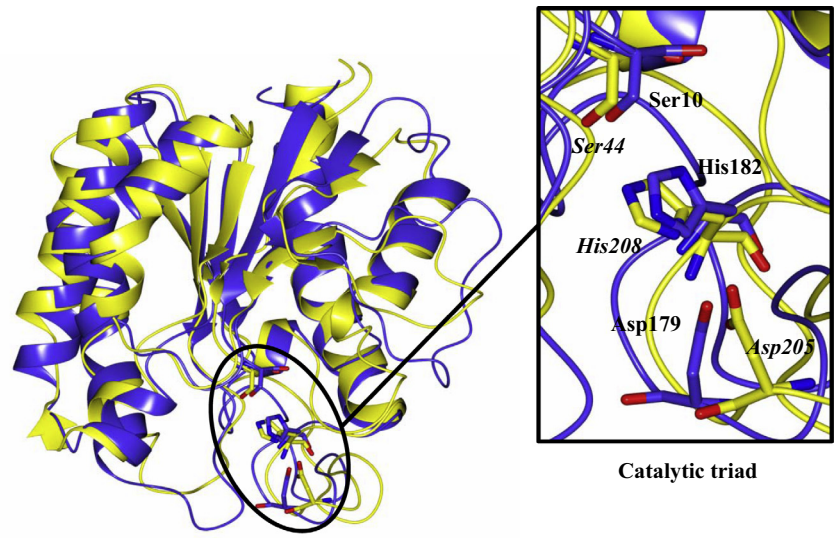

Fig. 2. Superimposed models of the TcAE206 and CtCes3-1 structures. Each enzyme (TcAE206: blue, CtCes3-1: yellow) is shown as a ribbon model and both catalytic triads (Ser10–Asp179–His182 in TcAE206, Ser44–Asp205–His208 in CtCes3-1) are circled in black and shown as stick models. The atoms in the TcAE206 active site are colored as C: light blue, N: dark blue, O: red. The area around the catalytic triads is shown expanded and the 3-letter codes for the amino acids are provided (unitalicized, TcAE206 and italicized, CtCes3-1).

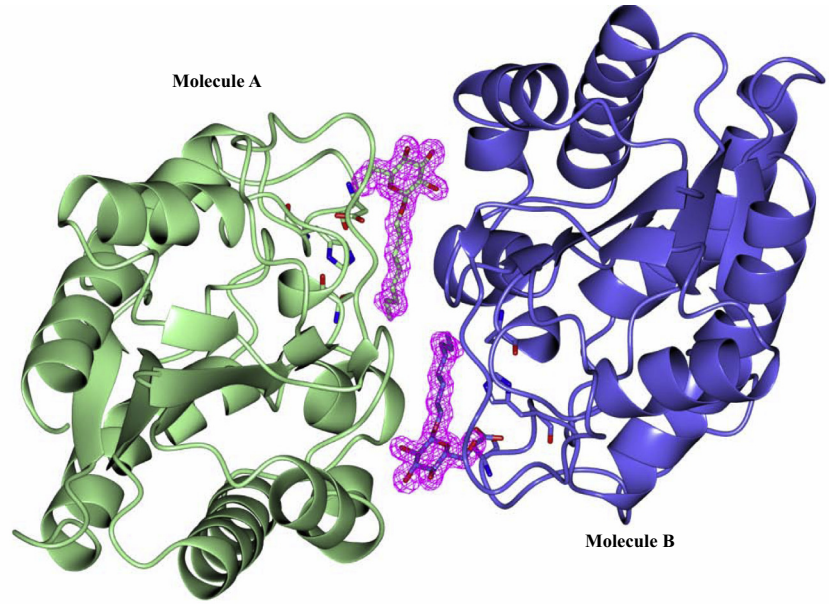

Fig. 3. Two β-OG molecules are located face to face in two molecules of TcAE206 with twofold axis symmetry in the crystallographic structure. Molecule A and B of TcAE206 are shown as ribbon models. Each β-OG and the catalytic triad residues (Ser10, Asp179 and His182) are shown as stick models. The 2Fo–Fc electron density map contoured at 1.0 is shown for β-OG. (Molecule A, O atoms: red; N atoms: blue; C atoms: light green/Molecule B, O atoms: red; N atoms: blue; C atoms: dark blue).

fungal CE3s (Fig. 1). However this bond was not observed at the active site of CtCes3-1, in spite of the high similarity of the crystal structure. The catalytic triad (Ser10, Asp179 and His182) of TcAE206 is conserved and corresponds to the catalytic triad in other SGNH hydrolases. Interestingly, the crystal structure shows a β-OG molecule, a detergent in the crystallization mixture, closely bound near the catalytic triad and filling the cavity. However, no significant interactions were observed between β-OG, Ser10, Asp179 and His182 in the active site. The lack of strong interactions between β-OG and the catalytic triad suggests that β-OG bound in the active site accidentally and contributed to stabilizing crystal packing. TcAE206 is prepared and produces as monomer protein. However, two molecules of TcAE206 are located with twofold crystallographic symmetry in the unit cell (Fig. 3). Furthermore, two active sites, each containing one molecule of β-OG, are located face to face in the unit cell. One would expect a pyranose-containing ligand to be oriented in a position that could indicate the hydroxyl preferentially deacetylated. Analysis of the protein complexed with the substrate will be needed to determine whether this conformation is dependent on β-OG, or whether this conformation is similarly formed when the substrate is bound at the catalytic site.

Activity assays were conducted using three mutants (S10A, D179A, H182A) in which each residue in the catalytic triad was individually mutated to alanine. Replacement of Ser10 (which serves as the nucleophilic residues) resulted in the lowest activity compared with wild-type (Table 2). In contrast, alanine replacement of His182 (which serves both as an acidic and basic residue)

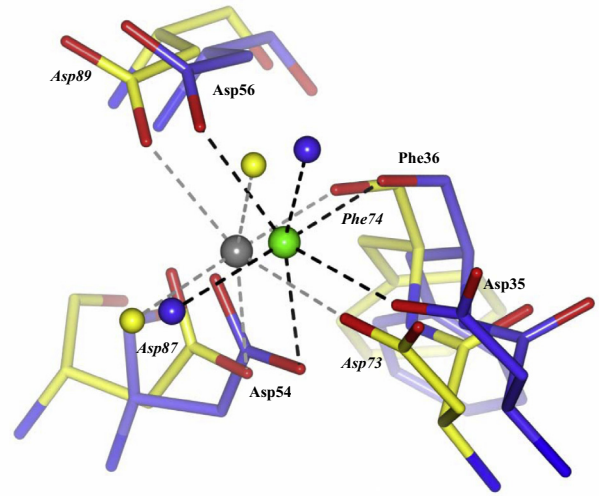

Fig. 4. Comparison of the calcium-binding site in TcAE206 and CtCes3-1. The final refined coordinates are shown for residues surrounding the calcium ion-binding site in TcAE206 and are superposed on the corresponding residues in CtCes3-1. The TcAE206 and CtCes3-1 residues are shown in 3-letter unitalicized and italicized code, respectively. The residues are shown as stick models, and the water molecules and calcium ions are represented as spheres. The hydrogen bonds are shown as black dashed lines (TcAE206) and gray dashed lines (CtCes3-1). The color scheme is: TcAE206: O atoms: red; N atoms: dark blue; C atoms: blue, Water molecules: dark blue sphere; Calcium ion: green sphere; CtCes3-1: O atoms: red; N atoms: blue; C atoms: yellow; Water molecules: yellow spheres; Calcium ion: gray sphere.

or Asp179 (which regulates the basicity of the histidine) resulted in little change in activity compared with wild-type (Table 3). Other study reported that the alanine substitutions of Ser and Asp were critically inactivated [35], but this case is different.

The crystallographic data obtained here show that the solvent-accessible cavity in the catalytic site of TcAE206 is rarely different from that of CtCes3-1. In addition, the loop region (Glu13–Arg18) near the active site of TcAE206 shortens 6 amino acids length compared with CtCes3-1 (Glu47–Arg58). TcAE206 and other fungal CE family 3 enzymes have a disulfide bond in the N-terminal region, located near the catalytic serine. CtCes3-1 lacks this S—S bond. Since this is the first disulfide bond to be characterized in a CE family 3 esterase, our findings offer new insights into the different catalytic mechanism of acetylesterase.

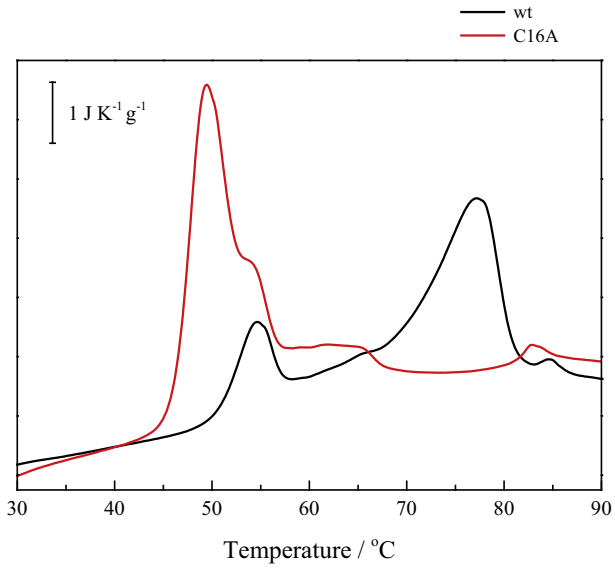

Fig. 5. DSC results. The DSC curves for WT and the C16A mutant in TcAE206 are shown (WT: black line; C16A: red line). Both protein concentrations were 1.0 mg/mL and dialyzed against 50 mM sodium acetate buffer (pH 5.5) before the DSC measurements. Bar represents heat capacity (1 J K^{-1} g^{-1}).

3.6. Calcium-binding site

Significant electron density corresponding to a ligand is observed above the N-terminal end of the central β-strand (β2). The ligand seems to be coordinated by the Asp35, Asp54 and Asp56 side chains, the main-chain carbonyl of Phe36, and two water molecules between 2.3 Å and 2.5 Å from the ligand (Fig. 4). CtCes3-1 coordinates a calcium ion through these residues [17], which are conserved in TcAE206; therefore, we speculate that the ligand in the corresponding site of the TcAE206 crystal structure is also a calcium ion. It is generally accepted that a divalent metal ion such as Ca^{2+} does not play an important role in the enzymatic activity of other CE family members (including CE3). But, other CE4 family, classified with aspartate metalloenzyme, is known to possess a divalent metal ion such as Zn^{2+} or Co^{2+} and these metal ions play an important role in the activity [9].

3.7. Influence of the S—S bond on function

To elucidate the function of the S—S bond (Cys16–Cys47) located near the active site, we prepared a mutant enzyme (C16A) lacking the S—S bond (Supplementary Fig. 1). From the structural analysis, it is clarified that there is no Cys residue near the S—S bond. Therefore, Cys47 in C16A dose not form S—S bond. C16A mutant exhibited dramatically lower enzymatic activity, about ninefold lower than that of wild-type (Table 3). DSC experiments showed that the Tm of C16A was drastically reduced to 50 °C as compared with 78 °C for wild-type (Fig. 5). These results indicate that the S—S bond plays an important role of the activity and thermostability, and that elimination of this bond prevents the mutant protein from adopting the correct structure. This suggests that the nucleophilic Ser10 in the catalytic triad supports the conformation required for activity due to the disulfide bond formed by Cys16–Cys47. The disulfide bond also helps stabilize neighboring areas, including a β-turn (β1) involving Ser10. The Ser10 of the C16A mutant may not aid recognition of the substrate to the same degree as Ser10 in the wild-type enzyme. This result suggests that C16A retains some activity, depending on how the substrate enters the cleft leading to the catalytic site.

Another type of esterase, feruloyl esterase (EC 3.1.1.73) belonging to the carbohydrate esterase family (CE family 1) is known to cleave the ester bond between ferulic acid and polysaccharides in plant cell walls. Feruloyl esterase belongs to the different family of AE (EC 3.1.1.72). The crystal structure of this enzyme from *Aspergillus oryzae* was recently solved and the structural information of the active site was elucidated [36]. The enzyme also has the same catalytic triad (Ser–Asp–His) as AE and the unique disulfide bond near the catalytic triad [36]. Present study shows the position of disulfide bond near the active site in TcAE206 is different from that of feruloyl esterase from *A. oryzae*. The crystal structure of AE from *Sinorhizobium meliloti 1021* has been solved recently [37]. However, no disulfide bond was observed near the catalytic triad of the enzyme. It was elucidated that the disulfide bond in TcAE206 forms the unique structure of the active site for serine hydrolase and seems to stabilize the position of Ser10 that is important for the substrate specificity of the enzyme.

4. Note

Coordinates and structure factors for TcAE206 have been deposited at the Protein Data Bank under the accession code 3X0H.

Conflict of interest

The authors declare no conflict of interest.

Acknowledgments

The X-ray diffraction data were obtained at the beam line BL44XU at SPring-8, Hyogo, Japan with the approval of the Institute for Protein Research, Osaka University, Osaka, Japan (proposal No. 2014A6903).

Appendix A. Supplementary data

Supplementary data associated with this article can be found, in the online version, at http://dx.doi.org/10.1016/j.febslet.2015.03.020.

References

[1] Kumar, R., Singh, S. and Singh, O.V. (2008) Bioconversion of lignocellulosic biomass: biochemical and molecular perspectives. J. Ind. Microbiol. Biotechnol. 35, 377–391.
[2] Biely, P. (2012) Microbial carbohydrate esterases deacetylating plant polysaccharides. Biotechnol. Adv. 30, 1575–1588.
[3] Brett, C.T. and Waldren, K. (1996) Physiology and biochemistry of plant cell walls (Black, M. and Charlewood, B., Eds.), Topics in Plant Functional Biology, vol. 1, Chapman and Hall, London.
[4] Sunna, A. and Antranikian, G. (1997) Xylanolytic enzymes from fungi and bacteria. Crit. Rev. Biotechnol. 17, 39–67.
[5] van den Brink, J. and de Vries, R.P. (2011) Fungal enzyme sets for plant polysaccharide degradation. Appl. Microbiol. Biotechnol. 91, 1477–1492.
[6] Deutschmann, R. and Dekker, R.F. (2012) From plant biomass to bio-based chemicals: latest developments in xylan research. Biotechnol. Adv. 30, 1627–1640.
[7] Christov, L.P. and Prior, B.A. (1993) Esterases of xylan-degrading microorganisms: production, properties, and significance. Enzyme Microb. Technol. 15, 460–475.
[8] Cantarel, B.L., Coutinho, P.M., Rancurel, C., Bernard, T., Lombard, V. and Henrissat, B. (2009) The Carbohydrate-Active EnZymes database (CAZy): an expert resource for glycogenomics. Nucleic Acids Res. 37, D233–D238.
[9] Taylor, E.J., Gloster, T.M., Turkenburg, J.P., Vincent, F., Brzozowski, A.M., Dupont, C., Shareck, F., Centeno, M.S., Prates, J.A., Puchart, V., Ferreira, L.M., Fontes, C.M., Biely, P. and Davies, G.J. (2006) Structure and activity of two metal ion-dependent acetylxylan esterases involved in plant cell wall degradation reveals a close similarity to peptidoglycan deacetylases. J. Biol. Chem. 281, 10968–10975.
[10] Pfeffer, J.M., Weadge, J.T. and Clarke, A.J. (2013) Mechanism of action of *Neisseria gonorrhoeae* O-acetylpeptidoglycan esterase, an SGNH serine esterase. J. Biol. Chem. 288, 2605–2613.
[11] Ghosh, D., Sawicki, M., Lala, P., Erman, M., Pangborn, W., Eyzaguirre, J., Gutierrez, R., Jornvall, H. and Thiel, D.J. (2001) Multiple conformations of catalytic serine and histidine in acetylxylan esterase at 0.90 A. J. Biol. Chem. 276, 11159–11166.
[12] Hakulinen, N., Tenkanen, M. and Rouvinen, J. (2000) Three-dimensional structure of the catalytic core of acetylxylan esterase from *Trichoderma reesei*: insights into the deacetylation mechanism. J. Struct. Biol. 32, 180–190.
[13] Topakas, E., Kyriakopoulos, S., Biely, P., Hirsch, J., Vafiadi, C. and Christakopoulos, P. (2010) Carbohydrate esterases of family 2 are 6-O-deacetylases. FEBS Lett. 584, 543–548.
[14] Li, X.L., Skory, C.D., Cotta, M.A., Puchart, V. and Biely, P. (2008) Novel family of carbohydrate esterases, based on identification of the *Hypocrea jecorina* acetyl esterase gene. Appl. Environ. Microbiol. 74, 7482–7489.
[15] Gutiérrez, R., Cederlund, E., Hjelmqvist, L., Peirano, A., Herrera, F., Ghosh, D., Duax, W., Jörnvall, H. and Eyzaguirre, J. (1998) Acetyl xylan esterase II from *Penicillium purpurogenum* is similar to an esterase from *Trichoderma reesei* but lacks a cellulose binding domain. FEBS Lett. 423, 35–38.
[16] Biely, P., Côté, G.L., Kremnický, L., Greene, R.V. and Tenkanen, M. (1997) Action of acetylxylan esterase from *Trichoderma reesei* on acetylated methyl glycosides. FEBS Lett. 420, 121–124.
[17] Correia, M.A., Prates, J.A., Brás, J., Fontes, C.M., Newman, J.A., Lewis, R.J., Gilbert, H.J. and Flint, J.E. (2008) Crystal structure of a cellulosomal family 3 carbohydrate esterase from *Clostridium thermocellum* provides insights into the mechanism of substrate recognition. J. Mol. Biol. 379, 64–72.
[18] Yamanobe, T., Mitsuishi, Y. and Takasaki, Y. (1987) Isolation of a cellulolytic enzyme producing microorganism, culture conditions and some properties of the enzymes. Agric. Biol. Chem. 51, 65–74.
[19] Mitsuishi, Y., Yamanobe, T., Yagisawa, M. and Takasaki, Y. (1987) Purification and properties of thermostable xylanases from mesophilic fungus strain Y-94. Agric. Biol. Chem. 51, 3207–3213.
[20] Watanabe, M. and Ishikawa, K. (2014) Crystallization and preliminary X-ray crystallographic analysis of a putative acetylxylan esterase from *Talaromyces cellulolyticus*. Acta Crystallogr. F Struct. Biol. Commun. 70, 1668–1670.
[21] Gill, S.C. and von Hippel, P.H. (1989) Calculation of protein extinction coefficients from amino acid sequence data. Anal. Biochem. 182, 319–326.
[22] Waters, D.M., Murray, P.G., Miki, Y., Martínez, A.T., Tuohy, M.G. and Faulds, C.B. (2012) Cloning, overexpression in *Escherichia coli*, and characterization of a thermostable fungal acetylxylan esterase from *Talaromyces emersonii*. Appl. Environ. Microbiol. 78, 3759–3762.
[23] Sakoda, M. and Hiromi, K. (1976) Determination of the best-fit values of kinetic parameters of the Michaelis-Menten equation by the method of least squares with the Taylor expansion. J. Biochem. 80, 547–555.
[24] McIlvaine, T.C. (1921) A buffer solution for colorimetric comparison. J. Biol. Chem. 49, 183–186.
[25] Otwinowski, Z. and Minor, W. (1997) Processing of X-ray diffraction data collected in oscillation mode. Methods Enzymol. 276, 307–326.
[26] Collaborative Computational Project, Number 4 (1994) The CCP4 suite: programs for protein crystallography. Acta Crystallogr. D50, 760–763.
[27] McCoy, A.J., Grosse-Kunstieve, R.W., Adams, P.D., Winn, M.D., Storoni, L.C. and Read, R.J. (2007) Phaser crystallographic software. J. Appl. Crystallogr. 40, 658–674.
[28] Gerrit, G.L., Serge, X.C., Victor, S.L. and Anastassis, P. (2008) Automated macromolecular model building for X-ray crystallography using ARP/wARP version 7. Nat. Protoc. 3, 1171–1179.
[29] Emsley, P. and Cowtan, K. (2004) Coot: model-building tools for molecular graphics. Acta Crystallogr. D60, 2126–2132.
[30] Murshudov, G.N., Skubák, P., Lebedev, A.A., Pannu, N.S., Steiner, R.A., Nicholls, R.A., Winn, M.D., Long, F. and Vagin, A.A. (2011) REFMAC5 for the refinement of macromolecular crystal structures. Acta Crystallogr. D67, 355–367.
[31] Laskowski, R.A., MacArthur, M.W., Moss, D.S. and Thornton, J.M. (1993) PROCHECK: a program to check the stereochemical quality of protein structures. J. Appl. Crystallogr. 26, 283–291.
[32] Potterton, L., McNicholas, S., Krissinel, E., Gruber, J., Cowtan, K., Emsley, P., Murshudov, G.N., Cohen, S., Perrakis, A. and Noble, M. (2004) Developments in the CCP4 molecular graphics project. Acta Crystallogr. D60, 2288–2294.
[33] Fujii, T., Koike, H., Sawayama, S., Yano, S. and Inoue, H. (2015) Draft Genome Sequence of Talaromyces cellulolyticus Strain Y-94, a Source of Lignocellulosic Biomass-Degrading Enzymes. Genome Announc. 3.
[34] Neumüller, K.G., de Souza, A.C., van Rijn, J.H., Streekstra, H., Gruppen, H. and Schols, H.A. (2015) Positional preferences of acetyl esterases from different CE families towards acetylated 4-O-methyl glucuronic acid-substituted xylo-oligosaccharides. Biotechnol. Biofuels 8, 7.
[35] Koseki, T., Miwa, Y., Fushinobu, S. and Hashizume, K. (2005) Biochemical characterization of recombinant acetyl xylan esterase from *Aspergillus awamori* expressed in *Pichia pastoris*: mutational analysis of catalytic residues. Biochim. Biophys. Acta 1749, 7–13.
[36] Suzuki, K., Hori, A., Kawamoto, K., Thangudu, R.R., Ishida, T., Igarashi, K., Samejima, M., Yamada, C., Arakawa, T., Wakagi, T., Koseki, T. and Fushinobu, S. (2014) Crystal structure of a feruloyl esterase belonging to the tannase family: a disulfide bond near a catalytic triad. Proteins 82, 2857–2867.
[37] Kim, K., Ryu, B.H., Kim, S.S., An, D.R., Ngo, T.D., Pandian, R., Kim, K.K. and Kim, T.D. (2015) Structural and biochemical characterization of a carbohydrate acetylesterase from *Sinorhizobium meliloti 1021*. FEBS Lett. 589, 117–122.
[38] Thompson, J.D., Higgins, D.G. and Gibson, T.J. (1994) CLUSTAL W: improving the sensitivity of progressive multiple sequence alignment through sequence weighting, position-specific gap penalties and weight matrix choice. Nucl. Acids Res. 22, 4673–4680.
[39] Gouet, P., Robert, X. and Courcelle, E. (2003) ESPript/ENDscript: extracting and rendering sequence and 3D information from atomic structures of proteins. Nucl. Acids Res. 31, 3320–3323.